New insights with optical coherence tomography in coronary bifurcation lesions treated with the Tryton and Cypher stent

Theodorus Blomen

promotor :
Prof. dr. Patrick WAGNER, Dr. Jo Dens

Universiteit Maastricht

Masterproef voorgedragen tot het bekomen van de graad van
master in de biomedische wetenschappen

universiteit hasselt

Contents

Contents....2

Abbrevations....3

Abstract....4

Introduction....5

- Atherosclerosis....5
  - Onset and development....5
  - Plaque instability....6
- Shear stress in bifurcations....8
  - Effects of shear stress that promote atherosclerosis....8
- Treatment of lesions in bifurcations....9
  - Bare metal stents....9
  - Drug eluting stents....10
- OCT....11

Materials and Methods....13

- Study design and endpoints....13
- Tryton and Cypher Stent....14
- OCT....15
- Statistics....18
- Medina Classification....19

Results....20

- In-Vitro results....20
- In-Vivo results....22
- Comparison of regions....24
- In Vitro and In Vivo results compared....26

Discussion....28

Conclusion....32

- Future....33

References....34

Abbrevations

Bif	Bifurcation
BMS	Bare Metal Stent
CTZ	Central Transition Zone
(L)CX	Left Circumflex Artery
CXCR	$G\alpha_i$ protein-coupled receptor
DES	Drug Eluting Stent
Dist	Distal(ly)
EBCT	Electron-Beam Computed Tomography
FD OCT	Frequency Domain Tomography
IVUS	Intravascular Ultrasound
LAD	Left Anterior Descending
LDL	Low Density Lipoprotein
MMP	Matrix Metalloproteinase
MV	Main Vessel
MVZ	(Proximal) Main Vessel Zone
OCT	Optical Coherence Tomography
PCI	Percutaneous Coronary Intervention
PIU	Probe Interface Unit
Prox	Proximal(ly)
QCA	Quantitative Coronary Angiography
SB	Side Branch
SBZ	(Distal) Side Branch Zone
SD	Standard Deviation
SLD	Superluminescent Diode
SMC	Smooth Muscle Cells
TCFA	Thin Cap Atheroma
TD OCT	Time Domain Optical Coherence Tomography
TF	Tissue Factor
VCAM	Vascular Cell Adhesion Molecule

Abstract

Aims:

A prospective analysis, to define with optical coherence tomography (OCT) the number of malapposed and free floating struts at the neocarina in coronary bifurcated lesions and to compare in-vitro and in-vivo data, in a model and coronary bifurcated lesions, using a Tryton and a Cypher stent (double stenting technique).

Methods:

In the in-vitro model the Tryton stent was deployed into the side branch followed by deployment of a Cypher stent in the main branch. Kissing balloon inflation was performed with a 3.0 and 2.5 mm balloon at 16 atmospheres, followed by OCT in the side branch and the main vessel (two pullbacks). The same strategy was used in 10 consecutive patients, with a coronary bifurcation lesion. The in-vivo balloons were sized according to the vessel diameter. The number of struts with malappostion, the number of free floating struts and the correlation in-vivo and in-vitro were calculated.

Results:

At the neocarina, per millimeter pullback, the percentage of malapposed and floating struts, coming from the main vessel and side branch respectively, is 9.4-12.9%. Compared to the segments proximally (1.8%) and distally (1.8%) to the carina, this difference is significant ($p < 0.03$). The numbers of malapposed and free floating struts in-vivo and in-vitro, at the carinal level, correspond well ($R^2 = 0.44$ and 0.98).

Conclusion:

In-vivo OCT correlates well with the in-vitro model. In a 2 stent technique, malapposition and floating struts remain at the neocarina, despite the use of a dedicated bifurcation stent and systematic kissing balloon technique at 16 atmospheres.

Key words

Tryton stent, Cypher stent, bifurcation, OCT, malapposition.

Introduction

Atherosclerosis

Atherosclerosis, from the Greek words athere (gruel) and skleros (hard), is the narrowing and hardening (loss of flexibility) of the artery walls because of plaque buildup. Plaque is made up of low density lipoprotein (LDL), macrophages, smooth muscle cells, platelets, and various other substances. By narrowing of the blood vessel lumen it can restrict blood flow.
Rupture of an atherosclerotic plaque can induce the formation of thrombus (blood clot) which subsequently may block blood flow. Such a blood flow block will result in ischemic stroke or heart attack.

Onset and development

Under normal conditions, endothelial cells of the arterial wall promote fibrinolysis and resist adhesion and aggregation of leukocytes. When activated by stimuli like smoking, hypertension, unhealthy diet, obesity, diabetes or inflammation, the endothelial cells begin to express a range of adhesion molecules induced by mediators such as proinflammatory cytokines, angiotensin II and oxidized lipoproteins. These mediators selectively recruit various leukocytes. Blood monocytes, which make up the biggest part of the inflammatory cells that populate plaques, adhere to the endothelial surface of the otherwise not expressed adhesion molecules. Upon monocyte adherence to the activated endothelium, proinflammatory proteins called chemokines provide a chemotactic stimulus that triggers the monocytes to enter the intima. As they settle in the intima, monocytes mature into macrophages. These macrophages display scavenger receptors on their outer membrane that allow them to bind to and engulf particles of lipoprotein. The cytoplasm becomes engorged with lipid

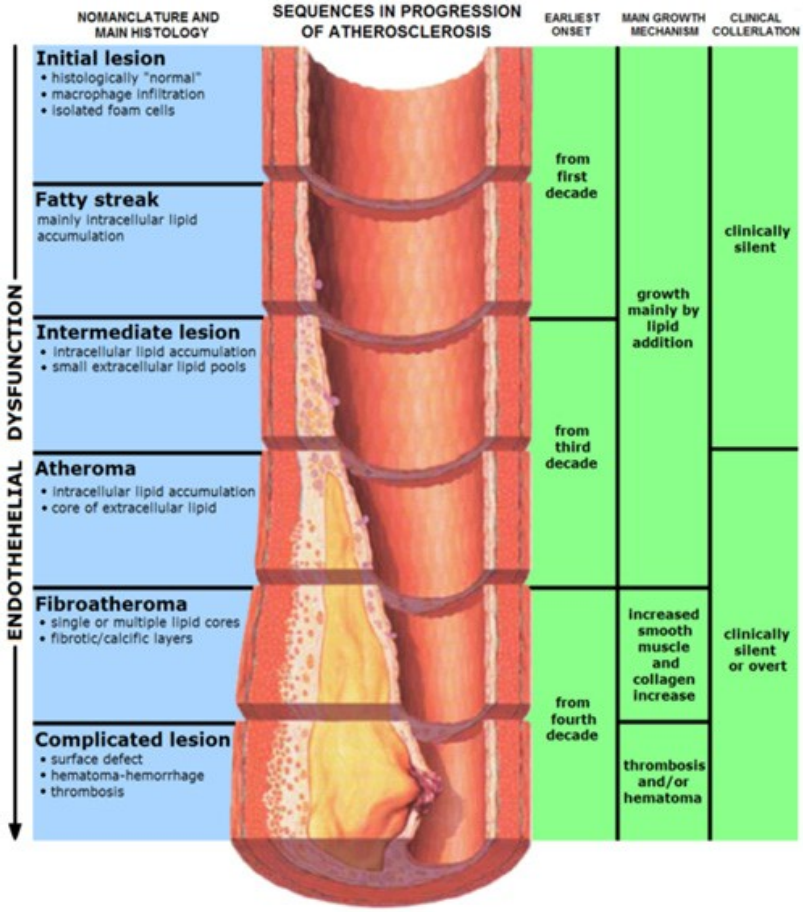

Figure 1: Various stages of atherosclerosis.

particles, which makes the macrophages become foam cells. The macrophages proliferate within the intima, sustaining and amplifying the inflammatory process by releasing several growth factors and cytokines, including enzymes that degrade the arterial extracellular matrix, like metalloproteinases, or MMPs, and the procoagulant tissue factor (TF). [1-4]

In addition to macrophages atherosclerotic plaques also contain a small population of T-lymphocytes of the adaptive immune response. Although they are less tnumerous than the macrophages, they appear to have decisive regulatory roles by instructing the more abundant monocytic effectors of the innate immune response. B-lymphocytes seem to have a inhibitory effect on atherogenesis, something that is being explored to develop vaccines against atherosclerosis. [5]

Plaque instability

Most cases of myocardial infarction are being caused by the rupture of a plaque's fibrous cap and its subsequent thrombosis.[6-7] Inflammation plays a role in the fragility of the fibrous cap as well as the thrombogenic potential. In addition to macrophages, T-lymphocytes play an important role in the inflammatory process leading to thrombosis. T-lymphocytes enter the intima (by binding VCAM-1 in response to various chemokines. [8-9]These chemokines bind to the chemokine receptor CXCR3, which is expressed on T-lymphocytes in the plaque. When activated in the intima, T-lymphocytes produce pro-inflammatory cytokines, including the CD40 (commonly found on T-lymphocytes) ligand, CD154. Ligation of CD40 by CD 154 induces the production of extracellular

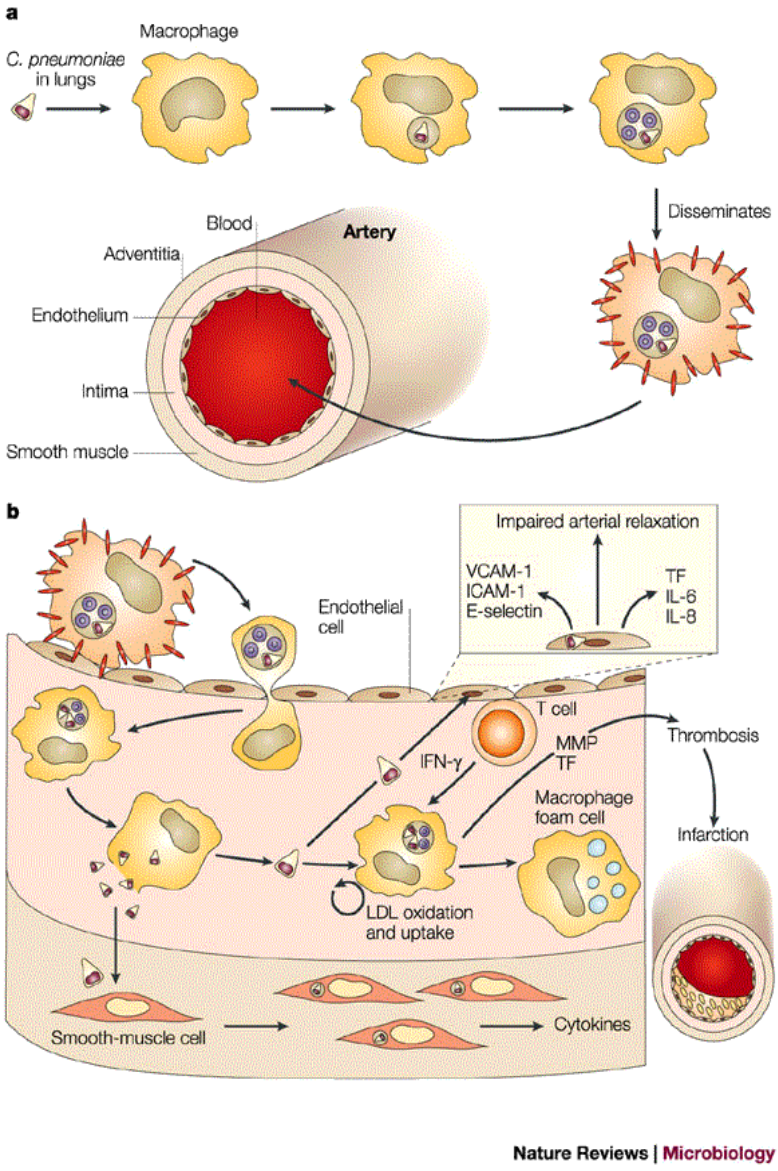

Figure 2: Onset and progress of the atherosclerotic plaque

matrix degrading MMPs, and the potent procoagulant TF [10-11]. TF initiates the coagulation cascade, enhancing the thrombogenicity of the plaque's lipid core. Inflammation also influences the metabolism of collagen, the key extracellular matrix molecule that supplies strength and stability on the fibrous cap. IFN-γ, which is produced by T-lymphocytes in the plaque inhibits production of collagen by smooth musle cells [12]. T-lymphocytes also promote collagen degradation indirectly by local production of cytokines, including CD40L, which boosts the elaboration of MMPs by neighboring macrophages. [10]

Adipose tissue, or body fat, does not only provide a storage depot for fat but can serve as a manufacturer of bioactive molecules, these molecules are also known as adipocytokines and they include proinflammatory cytokines. [13] Adipose tissue can elaborate numerous modulators of inflammation. [14] Visceral adipose tissue that accumulates in the abdomen drains directly through the portal circulation to the liver, where the proinflammatory cytokines, IL-6 in particular, modulate hepatic protein synthesis by evoking an acute phase response. Some acute phase reactants clearly participate in the causal pathway of thrombogenesis and thrombus formation and stability. For example, the clotting factor fibrinogen and plasminogen activator inhibitor-1 (PAI-1), an important inhibitor of fibrinolysis. [15-16]

When a fibrous cap of the fibroatheroma becomes thinner than 65 microns it is called 'thin cap atheroma' (TCFA), which is consedered as a precursor to acute plaque rupture. [17] The majority of coronary thrombi are associated with plaque rupture, of which TCFA is generally considered the precursor lesion. [18] Although most, if not all plaque ruptures are caused by TCFAs, plaque rupture is not the only mechanism of coronary thrombosis. Plaque erosion accounts for a small percentage of acute coronary thrombi, particularly frequent in younger patients. The precursor lesion of plaque erosion is unknown. [19-21] When a blood vessel is injured, as is the case in plaque rupture and plaque erosion, the body uses platelets and fibrin to form a blood clot to prevent bleeding. If thrombus fills more than 90% of a vessel lumen blood flow is prevented to such a degree that the tissue surrounding the vessel downstream from the clot are depraved of oxygen. Which results in infarction.

Shear stress in bifurcations

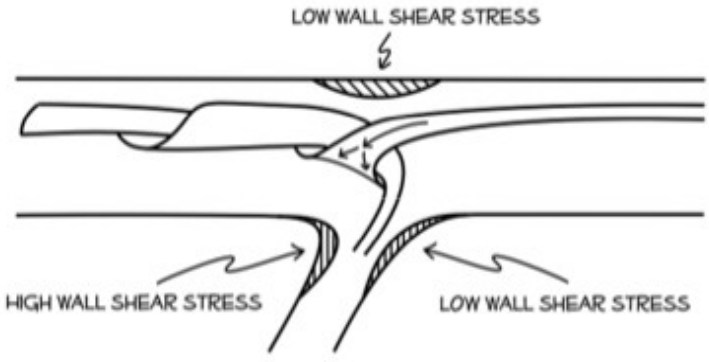

Figure 3: Flow patterns in the region of a branching vessel. When the side branch takes away more than 10% of the main vessel flow, causing secondary flow patterns and spatial variations in wall shear stress.

In the coronary arteries, flow is highly pulsatile, experiencing reversing flow in systole, and high forward flow in diastole. Also, in more than one plane, these arteries feature curvature. There is a high likelihood of low and oscillating wall shear stress, depending on the individual geometry. Bifurcated lesions are observed in 15-20% of patients undergoing a percutaneous coronary intervention (PCI). [22] Coronary bifurcations are extraordinary susceptible to atherosclerotic lesions because of the hemodynamic alterations that occur at branches in the arterial tree [Figure 3] [Figure 4].

Effects of shear stress that promote atherosclerosis

These areas of low-shear stress accelerate artherosclerotic development by modulation of gene expression, which includes the promotion of endothelial cell dysfunction, causing increased lipoprotein uptake, upregulation of leukocyte adhesion molecules and the transmigration of leukocytes through the endothelium. All these factors contribute to the development and progression of atherosclerosis. Cheng et al. [23] reported that upregulation of endothelial nitric oxide synthase was observed a high-shear areas using a cast-induced increased shear stress model in the mouse carotid artery. In a later study, Cheng et al. [24] showed elevated gene expressions of interleukin-6, C-reactive protein, intercellular adhesion molecules, vascular cell adhesion molecules and vascular endothelial growth factor in the low-shear area using the same model. This means that shear stress plays an important role in early plaque formation as well as its progression. A study by Perktold et al. [25] also showed that bifurcation angle variation also plays a central role, namely the larger the

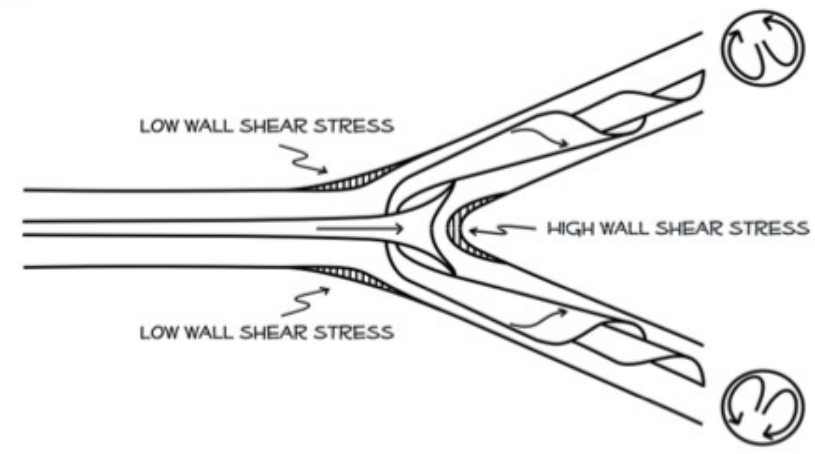

Figure 4: Flow patterns in the bifurcation. Fluid swirls into each of the branches causing spatial variations in wall shear stress.

angle of bifurcation, the greater the turbulence, the more susceptible of atherosclerotic development. There is in fact considerable variability in left main/LAD/Lcx geometries among patients. A study by Ding et al. [26] of 17 casts of this bifurcation showed a mean bifurcation angle (between LAD and Lcx) of 84.3 degrees, with a standard deviation of 14.2 degrees, and most notably, a range from 47.1 degrees to 107.1 degrees. Also, the ratio of the caliber from the proximal to the distal or side branch also influenced flow turbulence [27]

Treatment of lesions in bifurcations

The treatment of bifurcated lesions is technically more demanding since there is the risk of side branch occlusion and sometimes double stenting techniques are needed. Previous studies have shown that the use of 2 bare metal stents results in an unacceptable high rate of restenosis and repeat revascularization. [28] With the use of drug eluting stents (DES), the repeat revascularization rates, even with double stenting techniques remain below 6%. The side branch restenosis rate remains at 13%. [29] However in a two-stent strategy the risk of myocardial infarction remains higher. Dedicated bifurcation stents are being developed to decrease the risk of side branch occlusion and reduce the rate of side branch restenosis. One of these devices is the Tryton stent (Tryton Medical, Inc., Newton, MA, USA). The Tryton stent secures the side branch vessel. [30] A second stent is deployed in the main vessel, usually a drug eluting stent. For the purpose of the study the Cypher stent was used as a second stent.

Bare metal stents

Balloon angioplasty was widely performed for severely narrowed atherosclerotic coronary lesions during the first percutaneous coronary interventions. Limitations such as high rates of restenosis with early plaque recoil and late arterial shrinkage made the technique ineffective. [31-32]
Compared to conventional balloon angioplasty, the advent of coronary artery stents offeres much improved radial strength therefore, preventing both acute and chronic causes of narrowing resulting in reduced rates of acute arterial closure and restenosis. [33]
Unfortunately, when stenting was introduced it was accompanied by high frequencies of acute stent thrombosis and although a lot was improved in anti-platelet therapy and stent deployment methods, there are still minor non-occlusive adherent platelet/ fibrin thrombi to be found around stent struts reletively common in implants placed three days or less ago. [34] At 1 month after placement, platelets are no longer apparent, and fibrin usually becomes incorperated into the neointima. Acute inflammatory cells, mainly composed of neutrophils, are associated with stent struts and frequently present in early time periods, however, these cells are rarely observed beyond 1 month. [35] In contrast, chronic inflammatory cells such as macrophages and/or giant cells are present at all times as a foreigh body reaction to the stent itself since the exposure of stent struts is permanent.

After two weeks of stent implantation, the neointima consists primarily of smooth muscle cells and proteoglycans. Recognized pathological factors such as the degree of medial injury, inflammation, and strut penetration into the necrotic core are identified as predictors of restenosis resulting from excessive neointimal growth. [36] Moreover, re-endothelialization of the stented luminal surface is considered pivitol as a deterrant to stent throbosis and complete endothelialization is typically confirmed by 3 to 4 months in bare metal stents. [37-38]

Drug eluting stents

Although stents offered a big improvement over balloon angioplasty, restenosis was a new complication which was considered a major limitation with a prevalence as high as 20 to 30 percent. [39] Since the primary cause of restenosis is attributed to the excessive proliferation of smooth muscle cells, the development of new technologies mainly focussed on specific targets aimed at preventing neointimal hyperplasia. Real clinical success was reached with the advent of localized therapy using stents as a drug delivery platform. [40] This method of sustaining drug delivery takes advantage of polymers to attach and promote controlled elution of drugs from the stent. The RAVEL clinical trial eventually produced a magnificent zero percent stenosis. [41]
The local delivery of cytostatic or cytotoxic drugs using a stent based technology has reduced restenosis after PCI impressively. [42] Currently, polymer-based sirolimus and paclitaxel-eluting stents are twidely used. Despite the goal of preventing mitogen-induced smooth muscle cell proliferation, the early preclinical studies showed these drugs to markedly delay arterial healing characterized by persistent fibrin deposition and poor luminal surface endothelialization. Further it is evident from pre clinical studies that with continued implant duration there is improved arterial healing with a return of neointimal growth and absence of long-term effects [43].
Re-endothelialization following BMS implantation in the coronary circulation is near complete by 3 to 4 months whereas for DES it is projected to take much longer. Moreover, other indications instenting such as longer lesion lengths ofter require,overlapping DES which may further impair re-endothelialization. As proof, overlapping pairs of Cypher or Taxus stents were implanted in rabbit iliofemoral arteries and subsequently en face examened by scanning electron microscopy. These studies demonstrated markedly delayed re-endothelialization at 28 days, in particular at sites of stent overlap, which was persistent up to 90 days of implantation. [44]

OCT

After stents are placed to secure blood flow in a previously narrowed vessel contrast can be added to the blood and susequent X-ray imaging will show whether blood flow has been restored. To see if a stent is placed optimally against the vessel wall, intravascular imaging is necessary. A new technique to do so is optical coherence tomography. Optical coherence tomography is an optical signal acquisition and processing method. It captures up to sub-micrometer-resolution, three-dimensional images from within optical scattering media like biological tissue. [45] OCT is based on low coherence interferometry, typically employing near-infrared light, which is non-radiant as opposed to x-rays. The use of relatively long wavelength light allows it to penetrate into the scattering medium. In conventional interferometry with long coherence length like laser interferometry, interference of light occurs over a distance of meters. In OCT, this interference is shortened to a distance of micrometers, by the use of broadband light sources. Light with broad bandwidths can be generated by using superluminescent diodes or lasers with extremely short pulses (femtosecond lasers). [46]

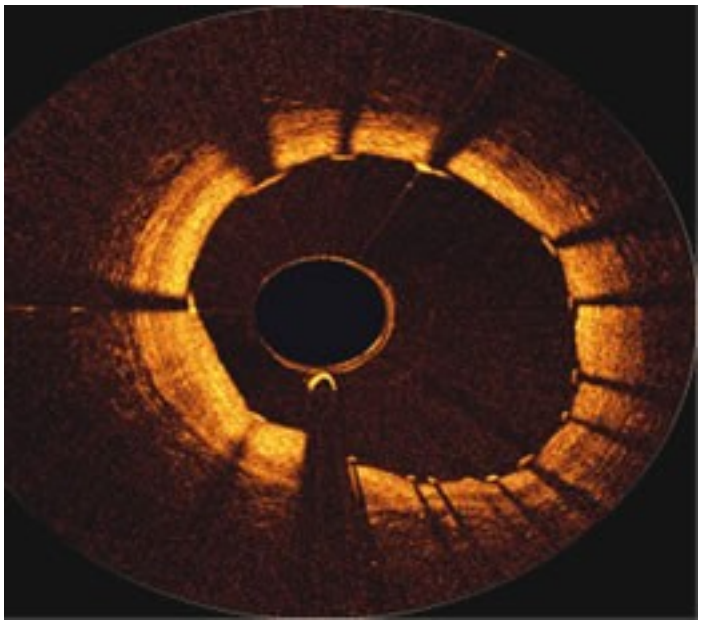

Figure 5: A typical OCT image. The dark circle in the centre is the imaging probe itself inside the lumen. The bright yellow ring around it is the vessel wall. Stent struts can be seen as bright yellow dots casting a cone shaped shadow towards the outer edges of the image, these shadows occur because the near infrared light can not penetrate the metal struts. The slightly bigger yellow object directly adjecent to the imaging probe is the guiding wire on which the probe was mounted.

The light in an OCT system is divided into two parts by the interferometer. The sample beam which directs light through the fibre-optic imaging wire into the biological tissue (or sample) and collects the backscattered light and the reference beam which is usually reflected upon a reference moving mirror. Because the light from the sample beam and the light from the reference beam travel an equal distance (a difference of less than a coherence length), the combination of the two in the detector is used to generate an interference pattern or interferogram. In Time Domain Optical coherence tomography (TD OCT), a reflectivity profile of the sample can be obtained by scanning the mirror in the reference beam. Areas of the sample that reflect back a lot of light will create greater interference than areas that don't. Any light that is outside the short coherence length will

not interfere. This reflectivity profile, called an A-scan, contains information about the spatial dimensions and location of structures within the item of interest. A cross-sectional tomograph (B-scan) may be achieved by laterally combining a series of these axial depth scans (A-scan).

In Frequency Domain (also called Fourier Domain) Optical coherence tomography (FD OCT) the broadband interference is acquired with spectrally separated detectors, either by encoding the optical frequency in time with a spectrally scanning source or with a dispersive detector, like a grating and a linear detector array. The depth scan can be immediately calculated by a Fourier-transform from the acquired spectra, without movement of the reference beam. This feature improves imaging speed dramatically, while the reduced losses during a single scan improve the signal to noise proportional to the number of detection elements. The parallel detection at multiple wavelength ranges limits the scanning range, while the full spectral bandwidth sets the axial resolution.[45-46]
Optical coherence tomography (OCT) allows clear visualization of the stent struts and should give an answer if the Tryton stent, combined with the Cypher stent, provides good stent apposition at the level of the carina of the bifurcation. More about OCT is explaned elsewhere.

For the aim of the study the number of free floating and malapposed struts at the carina are counted and in-vivo data are compared with in-vitro data.

Materials and Methods

Study design and endpoints

The in vitro model consisted of two plastic tubes, 3.0 and 2.0 mm in internal diameter, connected to each other in a 45° angle with glue. The Tryton Side-Branch stent is a cobalt-chromium stent designed for bifurcation lesions. It consists of three zones; the side branch zone (6 mm), the transition zone (4 mm) and the main vessel zone (8 mm). The strut thickness is 0.0033" (84 μm) (4). A 3.5/2.5 mm – 19 mm Tryton stent was deployed to the side branch followed by deployment of a 3.0 - 18 mm Cypher stent in the main branch. Kissing balloon inflation was performed with a 3.0 and a 2.5 mm balloon at 16 atmospheres, followed by OCT in the side branch and the main vessel (two pullbacks). A non-occlusive technique (Light Lab Imaging Inc. Westford, MA, USA), was used for image acquisition. A continuous flush was done in-vivo using a power injector. Pullback speed was set at 3 mm per second.

The same strategy was used in 10 consecutive patients, who had an indication for treatment of a coronary bifurcation lesion, and were included in the Tryton registry, which was approved by the ethical committee. A 7 F guiding was used. All patients were pretreated with acetylsalicylic acid and clopidrogrel. During the procedure Heparin 70 u/kg iv was used, with 35 U/kg added after 30 minutes. After predilatation of the main vessel and side branch, the Tryton stent was placed to the side branch. After recross with a wire and a balloon the Cypher was placed in the main vessel, followed by recross and kissing balloons (whenever possible at 16 atm). OCT was performed from the side branch to the proximal part of the bifurcation and from the distal main vessel to the proximal main vessel. 5 regions are defined; main vessel distal to the bifurcation, the carina (both in a side branch pullback and a main vessel pullback), main vessel proximal to the carina and the side branch.

The Cypher stent was used in all patients in order to have a uniform definition of maloppasition. Malappostion is defined as the strut-thickness (Cypher 154 μm) plus an additional 15 μm, since the spatial resolution of OCT is 10-20 μm. Floating was defined as twice the strut thickness plus an additional 15 μm for spatial resolution.

In-vivo and in vitro OCT data were compared to determine the number of struts per millimeter pullback with malappostion, and the number of free floating struts.

Quantitative coronary angiography (QCA) (Siemens Erlangen, Germany), was done off line to determine vessel sizes and residual stenosis. The bifurcation lesions were classified according the Medina classification.

Tryton and Cypher Stent

The Tryton side branch stent is a balloon expandable cobalt chromium bare metal stent (BMS) made up of three distinct zones (Figure ™). A distal side branch zone (SBZ), which is designed as a standard slotted tube stent as used on lesions in unbifurcated vessels. A central transition zone (CTZ), which is made up of three panels, equally spread from one another, capable of being deformed independantly. The central transition zone design allows for complete stent coverage of the ostium and suits a wide range of commonly encountered anatomical pathologies in bifurcated coronary vessels. The third zone, the proximal main vessel zone (MVZ), is composed of three panels that are associated with the three panels in the CTZ and these terminate proximally in a circumferential ('wedding') band. Upon placement of the Tryton stent in the side branch a Cypher DES is positioned in the main vessel with the proximal end placed inside the proximal region of the Tryton stent passing through the CTZ planes into the distal main vessel. After deployment of the Cypher stent, the side branch was recrossed to allow for simultaneous kissing balloon infl ation to be performed. [47]

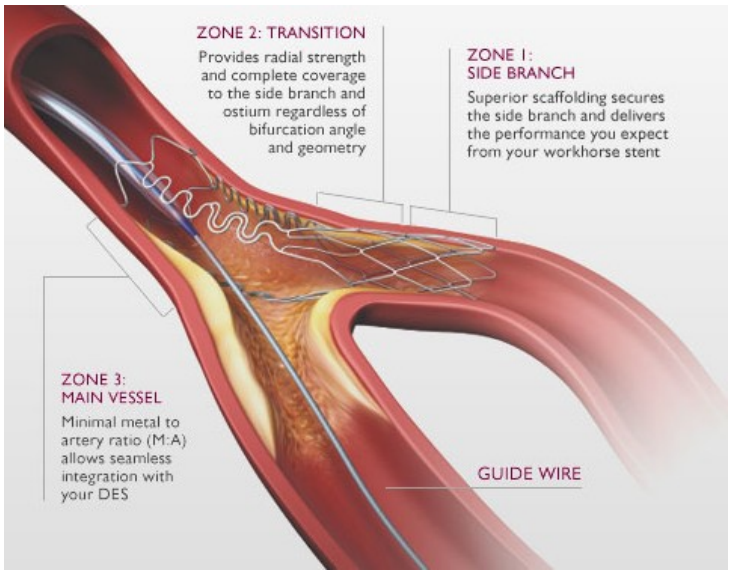

Figure 6: The Tryton side branch stent composed of three zones. 1) Side branch zone, scaffolding. 2) Central transisition zone, radial strength 3) Main vessel zone, minimal coverage

OCT

Intravascular ultrasound (IVUS) was introduced in the late 1980s as the first imaging technique that demonstrated the benefits of imaging inside the walls of coronary arteries. IVUS imaging works by employing a rotating ultrasonic transducer, or an array of fixed transducers, mounted at the tip of a catheter to obtain a cross-sectional view of the artery. Intravascular ultrasound is most oftenly used in clinical practice for stent measurements, plaque volume determination and calcium deposit localization. Current IVUS imaging systems have a resolution of 100 to 300 μm which is not sufficient to visualize the thin fibrous caps that are typical in plaques that are susceptible to rupture. Coronary angioscopy was also introduced in the 1980s, as a means of obtaining a clearer view of the artery. The angioscope is a miniature fiber optic endoscope that is threaded into the heart through a catheter. After the artery is briefly occluded with a balloon and flushed to remove the residual blood out of the field of view, the thrombus, plaque, arterial dissections and other vascular abnormalities can be viewed. Angioscopy does provide a rough indication of the composisition of the coronary lesion according to its morphology and color, however, it is not able to aid in the assessment of below-surface lesions. Angioscopy, as well as IVUS, is too invasive and expensive for general diagnostic screening and therefore it is mainly applied in studies that focus on the research and development of new interventional therapies. Electron-beam computed tomography (EBCT) is a relative newcomer to the coronary imaging field and it has recently gained popularity as a screening tool. In EBCT, X-rays are generated by steered electron beams and used to capture snapshots of the coronary arteries without having the patient undergoing invasive procedures like catherization. Risk assessment of coronary artery disease is established by the quantification of the degree of calcification of the arteries. Calcium scores provided by EBCT have no direct relationship to factors that underlie sudden cardiac death, yet high scores can encourage at-risk patients to undergo additional assessments. The potential of optical oherence tomography to be used as an intravascular imaging technology was recognized soon ather the first publication of OCT images of biological tissue. [45] Early studies demonstrated OCT's unique ability to resolve atherosclerotic lesions in microscopic detail, lesions that were believed to be prone to sudden rupture in particular [48-49]. Features of OCT that make it attractive for intracoronary imaging are the high resolution and the small size of the fiber-based imaging probes. Although healthy coronary arteries have walls that are only a fraction of a millimeter thick, highly stenosed arteries may have lumens redused to a diameter of less than 1 mm by thickening of the vessel wall. Because of its small dimensions, OCT is well suited to image these heavily narrowed vessels.

The OCT system consists of four main components: a high speed imaging engine, a computer with keyboard and display, a probe interface unit (PIU) and a coronary imaging probe. Inside the imaging engine, an efficient polorization diversity interferometer splits polychromatic light (emitted by a polarized superluminescent diode, or SLD) into reference and sample beams. The coherence length of the SLD yields a resolution in the radial dimension of about 15μm. The sample beam couples into the imaging probe through a motorized rotary fiber coupler inside the PIU. To permit longitudinal scanning of a blood vessel for the collection of three-dimensional image sequences, the PIU contains a motorized mechanism that pulls the optical fiber back within the transparant sheath of the OCT probe as the fiber rotates. A fraction of the light backscattered from the artery passes back through the imaging probe into the interferometer, where it mixes with a reference beam. The reference beam polarization is oriented along an axis that splits signal power equally between the two outputs of the polarization splitter. The orthogonally polarized signals are detected seperately and, after high speed digitization, filtered and demodulated by programmable digital circuits. To obtain a signal the magnitude of which does not depend on the polarization state of the light returning from the sample arm, the sum of their squared signal magnitudes is calculated. This kind of polarization diversity processing ensures that polarization changes caused by bending and rotation of the optical fiber in the sample arm do not create image artifacts. The position of the reference mirror determines the sampling depth in the tissue since interference occurs only when the optical distances traveled by the sample and the reference beams match within the coherence length of the source. To achieve its high frame rates required for coronary imaging, a multi-faceted, cam-shaped reflector with an air-bearing motor scans the reference arm path length. [50] The basic building block of the OCT imaging probe is the fiber optic imaging core, composed of a single-mode fiber with a microlens/beam deflector assembly at its tip. The imaging core, which is less than 0.4 mm in diameter, employs an advanced micro-lens assembly at its tip to focus and direct the sample beam. [51] The assembly consists of segments of fiber with refractive-index profiles tailored to achieve the desired beam focus. Because

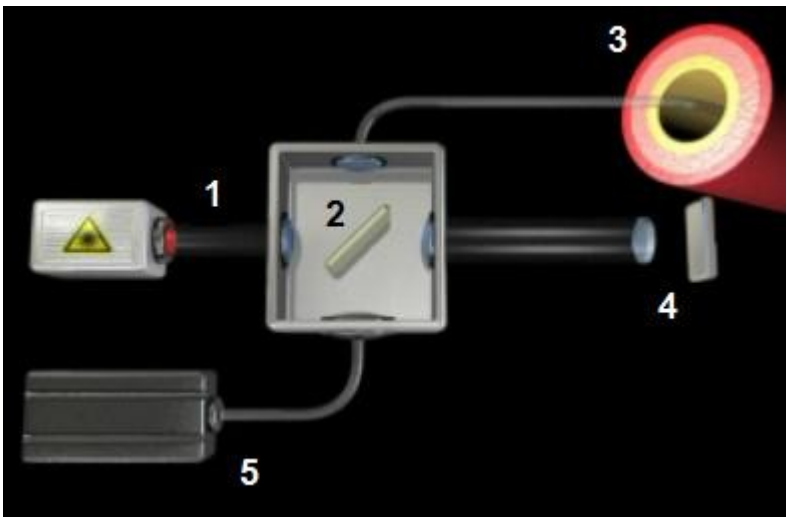

Figure 7: Near-infrared polychromatic light is emitted (1). An interferometer splits the light (2) and sends it to the tissue (3) and a reference path (4). After backscattering the two beams are recollected and an image is generated with software (5).

the fiber segments are fusion-spliced via arc welds, the assembly is similar to that of untraeted fiber. To deflect the focused beam perpendicular to the long axis of the fiber, one end of the distal coreless segment is polished at an angle close to 45 degrees. The lens focuses to a near diffraction-limited focal spot equal to 20-30 μm diameter at a working distance of 2 mm. Unlike rotary IVUS probes, the OCT imaging probe does not employ a torque cable. Instead, the optical fiber rotates and translates inside a plastic sheath that contains a specially formulated mixture of fluids. Eliminating the torque camble simplifies fabrication of the catheter (which reduces costs). A major challenge tot the use of OCT in coronary applications is the need to provide an efficient delivery system that enables the cardiologist to insert the OCT probe into the target artery and clear thestrongly scattering red blood cells from the field of view of the probe. Since blood from the heart of most patients can not be interrupted for more than 20 to 30 seconds, imaging must be accomplished within a short interval.

Examples of cathheter delivery systems designed for intracoronary OCT imaging include: 1) a monorail flush catheter, this catheter intgrates the imaging probe into a flush tube through which saline is injected with a syringe. The saline exits close to the aperture of the imaging probe. 2) An occlusion balloon catheter, an imaging probe with a spring mounted on its tip is inserted near the balloon through the guide wire lumen. Blood flow is interrupted briefly by inflating the balloon and flushing the residual blood from the target vessel before imaging. 3) An angioplasty balloon catheter, the aperture of the imaging probe is inserted under the balloon through the guide-wire lumen. Inflation of the balloon during the therapeutic angioplasty procedure displaces the blood between the probe and the wall of the artery. [50-51]

Statistics.

All statistic calculations were performed in NeoOffice Calc for Mac OSX.

From 10 patients we acquired 10 OCT pullbacks through the main vessel and 10 pullbacks through the side branch. The individual pullbacks were divided into a proximal data set that included all stent struts visable within 8 mm proximally from the start of the bifurcation, a bifurcation data set which included all stent struts over the entire length of the bifurcation and a distal data set including all stent struts within 8 mm distally from the end of the bifurcation. The 8 mm long scans that were the proximal and distal data all scans showing no stent struts were disregarded as it was because of an absence of stent material in that region. Indeed, no further stent matial was shown in the scans 'downhill' (proximally in the proximal scan, distally in the distal scan) the first frame that showed no stent struts. Furthermore, there was great variance in the ten measured neo-carinas even between the main vessel pullback and side branch pullback of the same patient. Because of this, all data was calculated per millimeter, so that statistical analysis could be made and graphics would be easier to interpret. The ten lengths of the neocarina in the MV pullback were compared to the lengths of the neocarina in the SB pullback with a one-tailed t-test for paired samples giving $p=0.045$. The proximal part of the main vessel and side branch is in fact the same. For this reason, only the results of the masin vessel pull back were included. Averages and standard errors were calculated for each region (proximal, bifurcation for main vessel, bifurcation for side branch, the distal part of the main vessel and the side branch itself) (Figure 1) per millimeter for total strut material, malapposed struts and in case of the neocarinas: floating struts. The 5 regions (Prox, Bif MV, Bif SB, Dist MV and Dist SB) were all compared to each other for total struts and percentage of malapposed + floating struts with two-tailed t-tests for paired samples (Table 1)(Table 2). Of the in vitro model the data was organized and converted in a similar way as the in vivo data. All regions were corrected for stend endings and the stent count was calculated per millimeter. Correlation co-efficients were calculated for the trend in total stent material and number of malapposed + floating struts. These findings were double checked by linear regression calculating the R-square value (Figure 8) (Figure 9).

Medina Classification

Depending on the distribution of the plaque in the segment of a coronary lesion in a bifurcation, a wide range of angiographic and anatomical morphologies are present. To define these lesions, many different classifications have been proposed, all defining each possible combination of lesions.

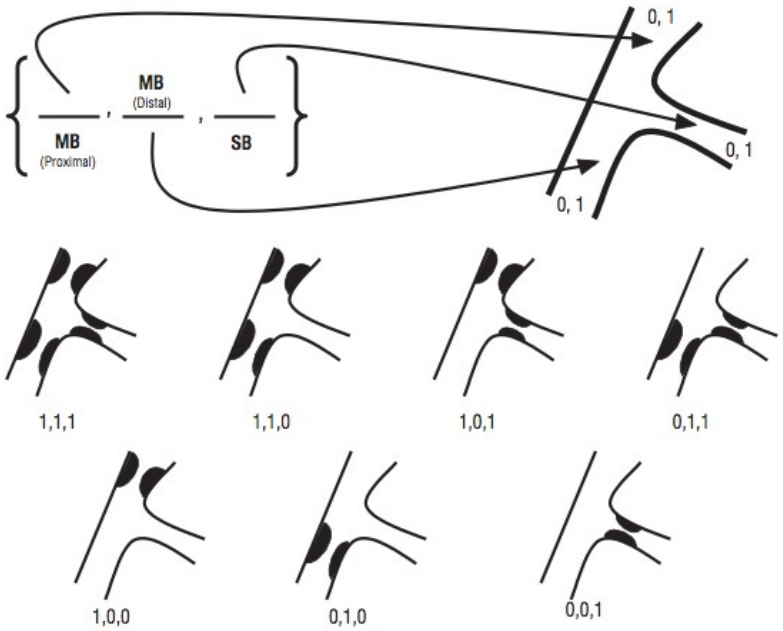

Figure 8: All possible combinations as described by the Medina classification.

The easiest classification is 'Medina', including all combinations and simply memorized.
The Medina classification makes use of the three components of a bifurcation; the main branch proximal, the main branch distal, and the side branch. In this sequence, an intuitive classification is made by giving each segment a binary value, 1 or 0, with 1 indicating that the segment is compromised and 0 indicating that there is no lesion present. [52]

Results

In-Vitro results

OCT analysis was done for 3 sections of the in vitro model. The definition of the 3 sections is illustrated in Figure 1.

Figure 2 represents the results of the analysis proximally to the bifurcation. Over a total length of 8 millimeters the total number of visible struts and the number of malapposed struts in the main vessel are given per millimeter: 41.25 struts per millimeter are visualized, of which 2.25 (5,5%) were in malapposition.

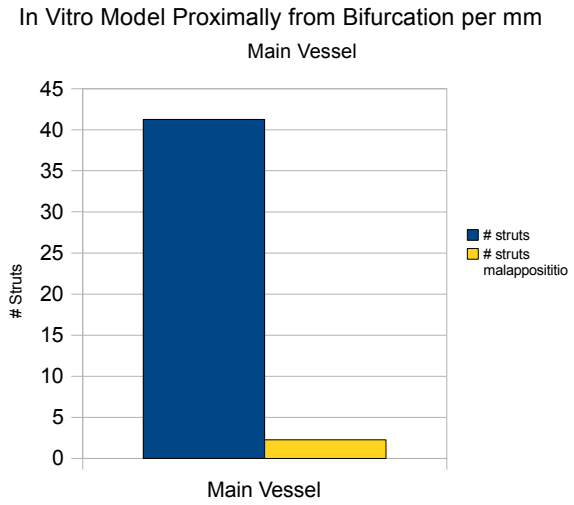

Figure 9: Number of stent struts proximally from bifurcation per millimeter

The cross section of the bifurcation is larger from the side branch than from the main vessel. The pullback from the side branch showed a bifurcation length of 4.8 millimeter whereas the pullback from the main vessel had a bifurcation length of 3.2 milimeter. The number of struts per millimeter from the side branch is 31.46 of which 1.88 (6%) were in malapposition and 10.42 (33%) were floating (Figure 3). Performing the pullback from the main vessel, there were 37.5 struts per millimeter visible of which none (0%) were in malapposition and 14.06 (37.5%) were floating per millimeter. By floating it is meant that the strut is in malapposition in the absence of a vessel wall ('tube' wall in case of the in vitro model). Floating was defined as twice the strut thickness plus an additional 15 µm for spatial resolution.

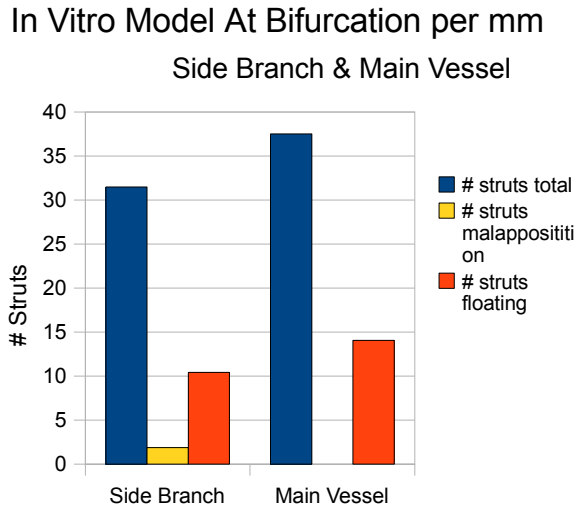

Figure 10: Number of stent struts at the bifurcation per millimeter

In a total length of 8 milimeters distally from the bifurcation, in the main vessel, 35.96 struts per millimeter are counted of which 0.38 struts were in malapposition. In the side branch 25.00 struts per millimeter were present of which 10.71 (43%) were in malapposition. Overal there was about the same percentage of malapposition in al sections, namely 6% or less. In the bifurcation there was a high percentage of floating struts of about 35% or one 3rd of the total.

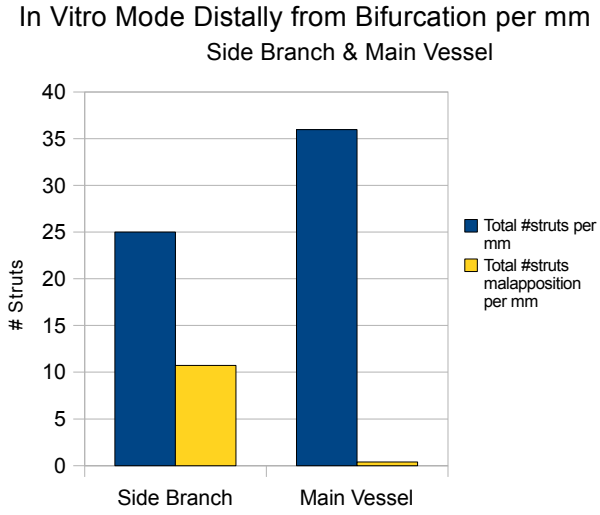

Figure 11: Number of stent struts distally from bifurcation per millimeter

In-Vivo results

Ten consecutive patients were treated according to the protocol. 60% were male, with a mean age of 68 years.

The target vessels were LAD and diagonal branch in 8, CX and lateral branch in 2.

The Medina classification for the bifurcation lesions was 1,1,1 in 10%, 1,1,0 in 10%, 1,0,1 in 10%, 0,1,1 in 30%, 0,1,0 in 30% and 0,0,1 in 10%. 5 patients had a stenosis of more than 50% in both the main vessel and the side branch.

All procedures were succesfull. QCA analysis showed a proximal reference vessel diameter of 3.45 mm ± 0.43, 2.85 mm ± 0.67 for the distal main vessel and 2.34 mm ± 0.38 for the side branch.

The residual stenosis after stenting was 0% for the proximal main vessel segment, 10.44% ± 10.88 for the distal main vessel segment and 18.79% ± 14.99 for the side branch

In Figure 5 the analysis proximally to the bifurcation is shown (main vessel). Over 8 millimeters the total number of visible struts and the number of struts in malapposition are given. OCT showed an average of 27.55 (SD 7.1) struts per millimeter. 0.49 (SD 0.43) (1.8%) of these struts were malapposed.

The bifurcation – as well as in the in-vitro model - is larger in the side branch than the main vessel (3.0 mm and 2.3 mm, p = 0.04). At the bifurcation, coming from the side branch, 30.0 (SD 16.19) struts per millimeter were visible. 0.6 (SD 1.35) (2%) were in malapposition, 3.28 (SD 4.8) (10.9%) were floating. Performing the pullback from the main vessel there were 35.44 (SD 12.8) struts visible, 0.48 (SD 0.84) (1.4%) were in malapposition, 2.98 (SD 4.6) (8.4%) were floating per millimeter. This small increase in the number of malapposed and free-floating struts performing the pull back from the side branch compared to the main vessel is not significant (p=0.34).

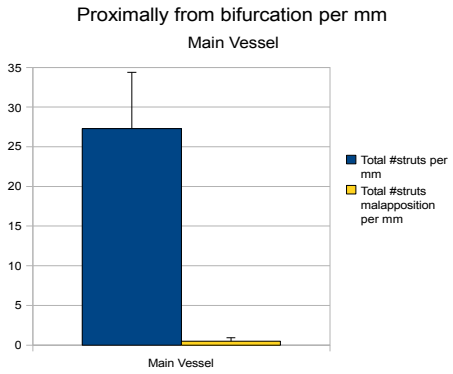

Figure 12: Number of stent struts proximally from bifurcation per millimeter

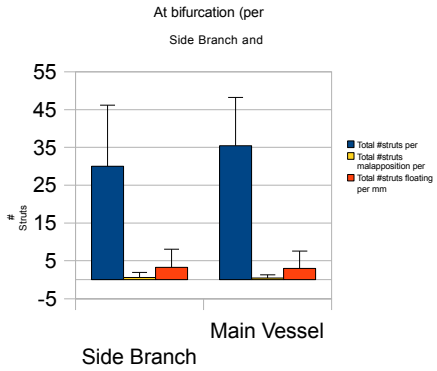

Figure 13: Number of stent struts at the bifurcation per millimeter

Figure 7 shows the results over 8 millimeters between the bifurcation and the distal part of the vessels. On average 22.61 (SD 7.68) struts per millimeter were counted in the side branch, 0.54 (SD 0.81) (2.4%) of these struts were malapposed. In the main vessel there was an average of 27.12 (SD 7.28) struts per millimeter, 0.49 (SD 0.77) (1.8%) of these struts were malapposed.

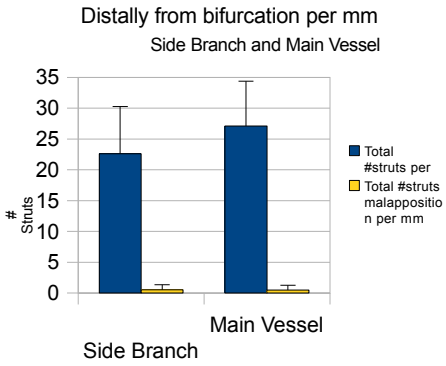

Figure 14: Number of stent struts distally from bifurcation per millimeter

Comparison of regions

All 5 regions were compared to each other to see wether there were differences in the amount of total stent material and/or percentage of malapposed stent struts.

Table 1: T-Tests for total stent material at different sections, prox = proximally, bif = bifurcation, dist =distally, SB = side branch, MV = main vessel

	Prox	Bif SB	Bif MV	Dist SB	Dist MV
Bif SB	0,42				
Bif MV	0,01	0,02			
Dist SB	0,12	0,01	0,001		
Dist MV	0,96	0,26	0,002	0,10	

Table 1 shows the p-values that indicate the difference of a region from another in terms of total stent material (average number of struts per mm). The bifurcation region for the main vessel pullback shows significantly more stent material than any of the other regions (p-values between 0.001 and 0.02). The bifurcation region for the main vessel even shows significantly more stent struts per millimeter than the 'same' region in the side branch pullback (p=0.02).

Table 2: T-Tests for percentage of malapposition and floating struts at different sections, prox = proximally, bif = bifurcation, dist =distally, SB = side branch, MV = main vessel

	Prox	Bif SB	Bif MV	Dist SB	Dist MV
Bif SB	0,02				
Bif MV	0,05	0,34			
Dist SB	0,53	0,03	0,10		
Dist MV	0,8	0,01	0,06	0,51	

Table 2 shows the p-values that indicate the difference of a region from another in terms of percentage of malapposed and floating stent struts combined.

The bifurcation for the side branch shows a significantly greater percentage of malapposed and floating material than any other region (p-values between 0.01 and 0.05) except for the 'same' region in the main vessel pullback (p=0.34). This bifurcation region of the main vessel pullback shows a significant higher percentage of malapposed and floating struts in comparison to the proximal region (p=0.05). Its p-values for the distal main vessel and side branch may be non-significant, but they are indeed small (p=0.06 and p=0.10).

Table 3 shows the p-values that indicate the difference of a region from another in terms of actual number of malapposed and floating stent struts combined. The bifurcation for the side branch shows a significantly greater number of malapposed and floating material than the 'same' region in the main vessel pullback (p=0.05). No other region differs significantly from another in number of malapposed and floating struts.

	Prox	Bif SB	Bif MV	Dist SB	Dist MV
Bif SB	0,13				
Bif MV	0,31	0,05			
Dist SB	0,71	0,13	0,32		
Dist MV	0,91	0,13	0,33	0,96	

Table 3: T-Tests for number of malapposition and floating struts at different sections, prox = proximally, bif = bifurcation, dist =distally, SB = side branch, MV = main vessel

In Vitro and In Vivo results compared

Table 4: Correlations for In Vitro and In Vivo results

		In Vitro	In Vivo	
		Total		Correl.
SB	Prox	36,63	26,6	
	Bif	31,46	30	0,59
	Dist	25	22,61	
MV	Prox	41,25	27,55	
	Bif	37,5	35,44	-0,19
	Dist	35,96	27,12	
		Malapp. + Float		
SB	Prox	0,38	0,24	
	Bif	12,3	3,88	0,66
	Dist	10,71	0,54	
MV	Prox	2,25	0,49	
	Bif	14,06	3,46	0,99
	Dist	0,38	0,49	

Table 4 represents the correlation co-efficiencies for total stent struts per region per pullback and total number of malapposed and floating struts per region per pullback between the In Vitro model and the patient (In Vivo) cases.
In the most left column it is stated whether it is the side branch (SB) pullback or the main vessel (MV) pullback. The column directly right of that states whether the numbers behind it are either the counts of the proximal (prox), bifurcation (bif) or distal (dist) region of that particular pullback, these scores are given per millimeter). Above the values is given if the scores are in-vivo or iv-vitro results and whether they represent total strut material or malapposed + floating struts. To the far right the calculated correlation co-efficient can be read.
In the side branch pullback, looking at total strut number, there was an correlation co-efficiency of 0.59. For the main vessel pullback the total strut number correlation co-efficiency was -0.19.
In the side branch pullback, looking at total number of malapposed and floating struts, there was an correlation co-efficiency of 0.66. For the main vessel pullback the number of malapposed and floating strut correlation co-efficiency was -0.99.

To present these correlations more simply, and to double check on our statistics, all data was put into graphs, displaying regression lines that give the square values of our correlation co-efficiencies (Figure 7, Figure 8, Figure 9, Figure 10).

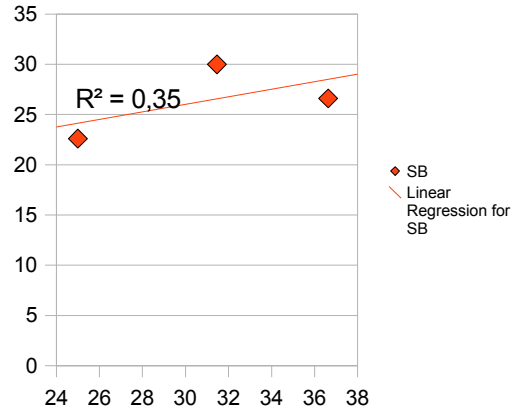

Figure 15: R-square value for total number of struts, side branch pullback

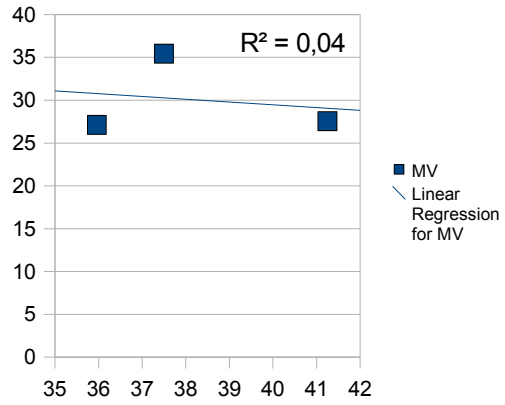

Figure 16: R-square value for total number of struts, main vessel pullback

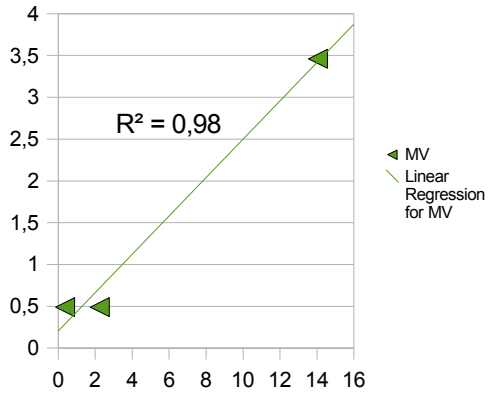

Figure 17: R-square value for number of malapposed and floating struts, main vessel pullback

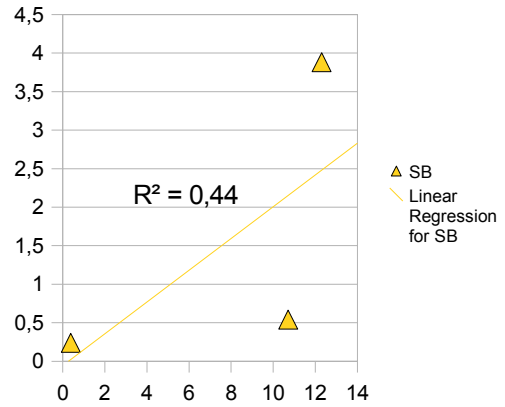

Figure 18: R-square value for number of malapposed and floating struts, side branch pullback

Discussion

The Tryton stent is a relatively easy to use device in treating bifurcation lesions. All procedures were successful. Our angiographic results were good and comparable with previous data (10-12), with a low residual stenosis in the main vessel (0% proximally and 10.4% distally from the bifurcation) and an acceptable residual stenosis (18.7%) at the side branch.

Overall, the in vitro model showed higher counts of stent material and higher percentages of malapposed and floating struts. These findings are likely to occur because of the unnatural, rigid composure of our experimental plastic model. Statistically, it is not possible to draw conclusions from one model simulation, although we have no reason to expect other results in further simulations with such a model. Our model did however show, overall, a good correlation with the in vivo findings when looking at the 5 regions and how they relate to one another in number of stent material and number of malapposed and floating struts combined. With the exception of total stent material in the proximal region, the in vitro showed the same tendencies as found in vivo, albeit in for bigger numbers.

The OCT data show, that proximally and distally from the bifurcation, the number of malopposed struts is low (1.8%). Proximally, a double layer stent is present (Tryton and Cypher), distally a single Cypher stent layer. Although these data are comparable, the high pressure kissing balloon inflation in the proximal part might have reduced the number of malopposed struts. On the other hand Tyczynski [53] looking at malapposition in the Tryton stent, reported more malopposition proximally (18.5%) to the bifurcation compared to the distal part (9.8%), despite the use of a kissing balloon technique. These authors did use however several other types of DES in the main vessel.

Our study was very conclusive in one way: although malapposition is not significantly higher in the neocarina, the combination with floating struts made up for a 5-fold of totally exposed bare metal stents in the lumen.

In respect to the comparisons of the 5 regions we defined earlier, the following was found: For total stent material we saw a significantly higher number of stent material in the bifurcation region of the main vessel pullback than all other regions. The bifurcation region for the side branch pullback was somewhat behind, showing no significant difference for 2 out of the 4 other regions. Discepancies between the side branch and main vessel pullback are discussed elsewhere.
Looking at percentages of stents that were malapposed or floating we found that the side branch pullback for the bifurcational region showed a higher incidence than any other region except for the 'same' region in the main vessel pullback. Although the 'main vessel bifurcation' did not show significantly higher percentages of malapposed and floating struts for the (distal) side branch and the distal main vessel it must be noted that the p-values were very close to significance ($p=0.10$, $p=0.06$).

We also looked at the number of malapposed and floating struts, which might be interesting since the actual number is more of an indication whether a stent is in danger of restenosis than a percentage is. Interestingly, the only regions to differ from each other in number of malapposed and floating struts were indeed the bifurcation regions of the main vessel pullback and the side branch pullback of that region. More about these differenced in pullbacks below.

Malapposition and free floating struts cannot be avoided at the neocarina. From bench studies, using a double stenting technique, incomplete stent expansion and compromised side branch access at the ostium, as well as crowding of metal became clear. [53] In-vivo IVUS data have shown small cross sectional areas at the side branch ostia. This incomplete stentexpansion, limited side branch access and excess of metal might predispose to restenosis and thrombosis. [54]The risk of thrombosis and restenosis is clearly higher after stenting of lesions located in bifurcations especially when a double stenting technique is used. [55] Malapposition and free floating metal struts ought to be the reason for the increased rate of stent trombosis. [56]
Our reported number (10-13%) of malopposed and free floating struts is lower compared to the previous report (33%). However it is clear from both reports that most malappostion and presence of free floating struts occur at the neocarina. Tyczynski also reported a larger wall to strut distance in the bifurcation, in the half towards the side branch. Since the authors performed a pull back from the main vessel only, information from the side branch was not available. Our OCT analysis was done for 3 sections of the in vitro model, divided into 5 regions. The definition of the 3 sections is illustrated in Figure 1.

Previous studies like that of Tyczynski calculated malapposition in the bifurcation for the main vessel pullback only. We found that the side branch pullbacks of our ten patients were significantly larger than in the main vessel pullbacks (p=0.045) at average lengths of 3.0 vs 2.3 mm. This phenomena is illustrated in Figure 18 and Figure 19. Because the OCT imaging probe is mounted onto the same guidinge wire to place the stent, the pullback is made in a natural curve inside the vascular lumen. This causes the neocarina to appear larger. Since previous studies performed only a main vessel pullback of the neocarina this might be of influence on their findings. We found a slight, however non-significant increase in malapposed and floating struts in the side branch pullback compared to the main vessel pullback. Future studies should access malappostion both from the main vessel as well as from the side branch.

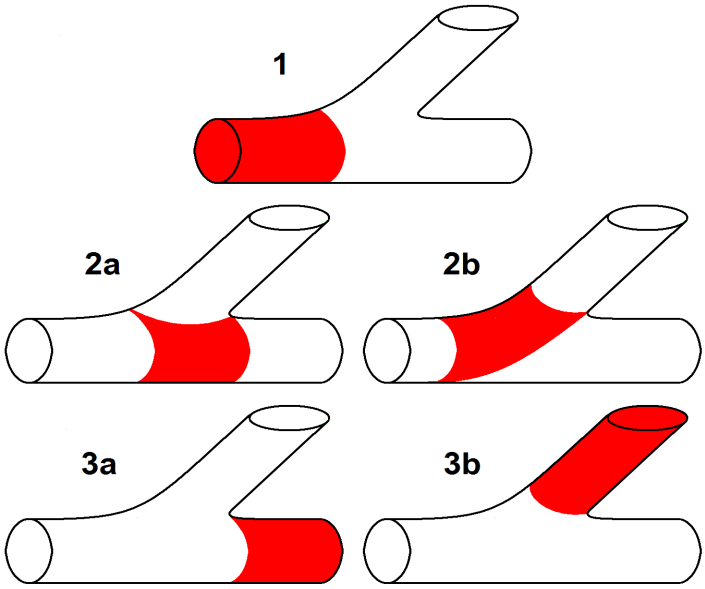

Figure 19: 3 sections of pullback: 1) proximal part of the main vessel, 2a-b) bifurcation for the main vessel and side branch respectivily, 3) distal part of a) main vessel and b) side branch.

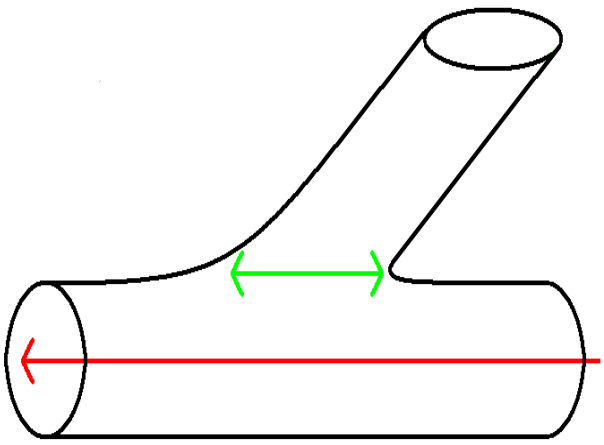

Figure 20: Main vessel pullback: the green arrow indicates the length of the neocarina as it appears in imaging

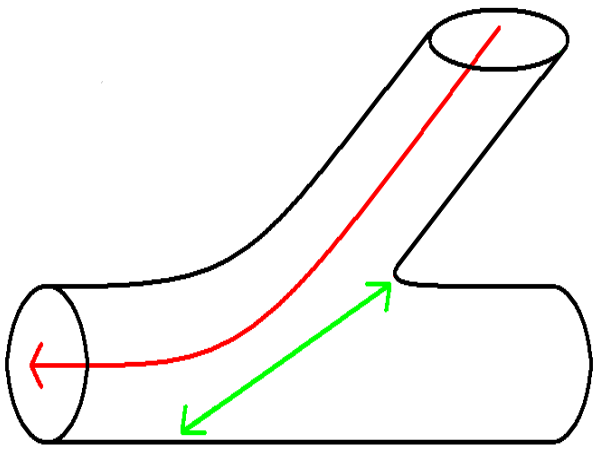

Figure 21: Side branch pullback: the green arrow indicates the length of the neocarina as it appears in imaging. Note that, because of the smooth curve a guiding wire makes, despite vessel diameters being the same the neocarina appears to be larger.

Kissing balloons, keeping their cylindric form, do not allow perfect circumferential appostion of the struts at the carina [57], as illustrated by Figure 20. Single short balloon inflations just at the carina or the use of a double wire single balloon ending in the distal main vessel as well in the side branch might perform better. However no clinical data are available. Finally other than Cypher stents in combination with the Tryton stent, might perform better or less good: direct comparisons are not available.

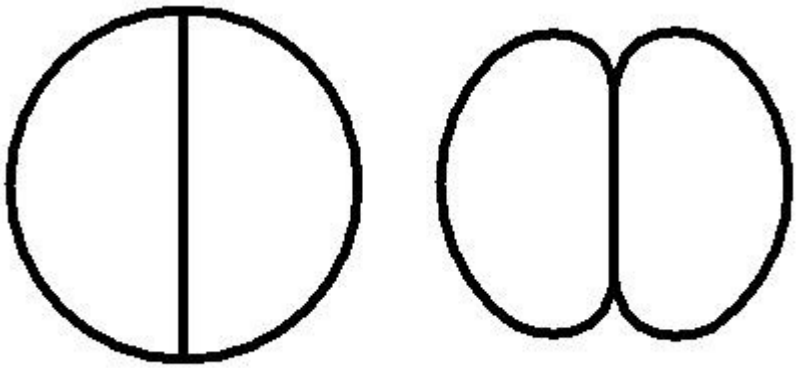

Figure 22: Ideally, two inflated kissing balloons would make a perfect circumferential expansion of the stent. In reality, kissing balloons hold some of their cylindric form when inflated, causing some stent material to be underexpanded.

OCT in-vitro and in-vivo, using the same stent delivery technique and kissing balloon inflations, showed a good correlation for the number of malopposed struts at the bifurcation. However the model can be improved: it should keep the same transparency so that it can be positioned easily without the use of X-rays, yet it also should by placed in a dense container after placement so that the near-infrared light undergoes enough scattering to make a well definable image. The model should be less rigid, comparable with the elastic characteristics of the vessel wall. Also, the bifurcation should make a smooth transistion from the main vessel to the side branch. Possibly, the models should be casted in mold for optimal smoothness, as opposed to glueing on tube on to another. In-vitro models that are made in such a way might allow studying the best performing combination of 2 stents, with the least malapposition.

Conclusion

We set out to compare in vitro and in vivo optical coherence tomography data. All procedures were successful. Our angiographic results were good and comparable with previous data, with a low residual stenosis in the main vessel and an acceptable residual stenosis at the side branch.
We found that there was good correlation overall between imaging in patients and our in vitro model. Malapposition was low in both in vitro and in vivo, whilst both also showing a peak of floating struts at the site of bifurcation. Unfortunately, we were not succesful in making a perfectly suitable model that approximated natural vascular conditions optimally. Our model was too rigid, causing struts to be malapposed excessively and our sites of bifurcation were to rough at the interface of the 'main vessel' and the 'side branch'. Luckily, there were more conclusions to be drawn from the in vivo data than we anticipated beforehand.

It was interesting to find great differences between the side branch pullback and the main vessel pullback when it comes to the bifurcation region. The simple fact is that since the imaging probe is mounted on the stent guiding wire, a pullback from the side branch will display a longer bifurcation region than a main vessel pullback because even if both vessels are (about) the same diameter, because of the natural curve that the guiding wire makes inside the lumen. Being this easily explained, it is that much remarkable that no previous studie came to such a conclusion. We have reason to believe that studies on malapposition, restenosis or plaque rupture in stent treatment of a bifurcated lesion may have different outcomes when adressing both the main vessel as well as the side branch in a pullback.

Optical coherence tomography showed to be a exciting new way of assessing the positioning and further situationing of stents after placement. It proved to be a user friendly imaging technique, both in acquiring the image as well as making use of the console to analyse and manage the data. Being a new intravascular imaging technique, some features of OCT are still missing, like automatic strut count in a frame and the assessment of floating struts by software. However, during our short study of just over half a year, multiple updates in fact took place and there is absolute guarantee that these missing features will eventually be standard. However, it is so far no big improvement compared to IVUS and replacing IVUS with OCT may be unnessecerily costly if one is not involved in a study that requires OCT.

Kissing balloons are not perfectly circumferential when inflated which causes some stent struts not to be optimally expanded against the vessel wall. Single short balloon inflations just at the carina or the use of a double wire single balloon ending in the distal main vessel as well in the side branch might perform better.

Future

Further studies is this field would be necessary to prove or disprove the use of the Tryton side branch in bifurcated lesions and the use of imaging by the OCT technique. In Vitro models should be more natural when it comes to flexibility and smoothness of the inner wall. In the assessment of stent material in the bifurcation a side branch pullback has to be made in addition to the main vessel pullback. If only to find out whether we were right that making only one pullback is of influence on the results. Bigger studies should be done to ensure the power of the findings. Because of the double stenting involved in bifurcated lesions, it would be interesting to see whether the kind of stents used or the technique of stenting makes a difference in malapposed and floating stents. The double stenting technique is not ideal, the double amout of stent material in the proximal main vessel is of particular concern. Perhaps there could be use in (partially) bio-degradable stents, in which case the double stent material, and its subsequent excessive presence of bare metal in contact with blood, would be temporarily.

References

1) Libby P. “Inflammation in atherosclerosis.” Nature 2002; 420: 868– 874.
2) Libby P, Ridker PM, Maseri A. “Inflammation and atherosclerosis.” Circulation 2002; 105: 1135 – 1143.
3) Mestas J, Ley K. “Monocyte-endothelial cell interactions in the development of atherosclerosis.” Trends Cardiovasc Med 2008; 18: 228 – 232.
4) Rader DJ, Daugherty A. “Translating molecular discoveries into new therapies for atherosclerosis.” Nature 2008; 451: 904 – 913.
5) Binder CJ, Horkko S, Dewan A, Chang MK, Kieu EP, Goodyear CS, et al. “Pneumococcal vaccination decreases atherosclerotic lesion formation: Molecular mimicry between Streptococcus pneumoniae and oxidized LDL.” Nat Med 2003; 9: 736 – 743. 22.
6) Kume T, Okura H, Yamada R, Kawamoto T, Watanabe N, Neishi Y, et al. “Frequency and spatial distribution of thin-cap fibroatheroma assessed by 3-vessel intravascular ultrasound and optical coher- ence tomography: An ex vivo validation and an initial in vivo feasibility study.” Circ J 2009; 73: 1086 – 1091.
7) Kashiwagi M, Tanaka A, Kitabata H, Tsujioka H, Matsumoto H, Arita Y, et al. “Relationship between coronary arterial remodeling, fibrous cap thickness and high-sensitivity C-reactive protein levels in patients with acute coronary syndrome.” Circ J 2009; 73: 1291 – 1295.
8) Mach F, Sauty A, Iarossi AS, Sukhova GK, Neote K, Libby P, et al. “Differential expression of three T lymphocyte-activating CXC chemokines by human atheroma-associated cells.” J Clin Invest 1999; 104: 1041 – 1050.
9) Heller EA, Liu E, Tager AM, Yuan Q, Lin AY, Ahluwalia N, et al. “Chemokine CXCL10 promotes atherogenesis by modulating the local balance of effector and regulatory T cells.” Circulation 2006; 113: 2301 – 2312.
10) van Wanrooij EJ, de Jager SC, van Es T, de Vos P, Birch HL, Owen DA, et al. “CXCR3 antagonist NBI-74330 attenuates atherosclerotic plaque formation in LDL receptor-deficient mice.” Arterioscler Thromb Vasc Biol 2008; 28: 251 – 257.
11) Mach F, Schoenbeck U, Bonnefoy JY, Pober J, Libby P. “Activation of monocyte/macrophage functions related to acute atheroma com- plication by ligation of CD40: Induction of collagenase, stromely- sin, and tissue factor.” Circulation 1997; 96: 396 –399.
12) Mach F, Schönbeck U, Sukhova GK, Bourcier T, Bonnefoy JY, Pober JS, et al. “Functional CD 40 Ligand is expressed on human vascular endothelial cells, smooth muscle cells, and macrophages: Implications for CD40-CD40 ligand signaling in atherosclerosis.” Proc Natl Acad Sci USA 1997; 94: 1931 – 1936.
13) Amento EP, Ehsani N, Palmer H, Libby P. “Cytokines and growth factors positively and negatively regulate intersitial collagen gene expression in human vascular smooth muscle cells.” Arterioscle Thromb Vasc Biol 1991; 11: 1223 – 1230.
14) Maeda K, Okubo K, Shimomura I, Mizuno K, Matsuzawa Y, Matsubara K. “Analysis of an expression profile of genes in the human adipose tissue.” Gene 1997; 190: 227 – 235.
15) Rocha VZ, Libby P. “The multiple facets of the fat tissue.” Thyroid 2008; 18: 175 – 183.
16) Gabay C, Kushner I. “Acute-phase proteins and other systemic responses to inflammation [Review].” N Engl J Med 1999; 340: 448 – 454
17) Yudkin JS, Kumari M, Humphries SE, Mohamed-Ali V. “Inflammation, obesity, stress and coronary disease: Is interleukin-6 the link?” Atherosclerosis 2000; 148:209-214 .
18) Burke AP, Farb A, Malcom GT, Liang YH, Smialek J, Virmani R. “Coronary risk factors and plaque morphology in men with coronary disease who died suddenly.” N Engl J Med. 1997; 336: 1276-82
19) Falk E, Shah PK, Fuster V. “Coronary plaque disruption.” Circulation. 1995; 92: 657-71.

20) Farb A, Burke AP, Tang AL, Liang TY, Mannan P, Smialek J, et al. “Coronary plaque erosion without rupture into a lipid core: a frequent cause of coronary thrombosis in sudden coronary death.” Circulation. 1996; 93: 1354-63.
21) Kolodgie FD, Burke AP, Farb A, Weber DK, Kutys R, Wight TN, et al. “Differential accumulation of proteoglycans and hyaluronan in culprit lesions: insights into plaque erosion.” Arterioscler Thromb Vasc Biol. 2002; 22: 1642- 8.
22) Virmani R, Burke AP, Farb A. “Plaque rupture and plaque erosion.” Thromb Haemost. 1999; 82 (Suppl 1): 1-3.
23) B. Meier et al. “Risk of side branch occlusion during coronary angioplasty.” Am J Cardiol 1984;53(1):10-14
24) Cheng et al. “Shear stress affects the intracellular distribution of eNOS: direct demonstration by a novel in vivo technique.” Blood 2005;106:3691-8
25) Cheng et al. “Atherosclerotic lesion size and vulnerability are determined by patterns of fluid shear stress.” Circulation 2006;113:2744-53
26) Perktold et al. “Pulsatile non-Newtonian blood flow in three-dimensional carotid bifurcation models: a numerical study of flow phenomena under different bifurcation angles.” J Biomed Eng 1991;13:507-15
27) Ding et al. “Influence of the geometry of the left main coronary artery bifurcation on the distribution of sudanophilia in the daughter vessels.” Arterioscl Thromb Vasc Biol 1997;17(7):1356-60
28) Richter et al. “Dynamic flow alterations dictate leukocyte adhesion and response to endovascular interventions.” J Clin Invest 2004;113:1607-14
29) P. Barlis et al. “Current and future developments in intracoronary optical coherence tomography imaging.” EuroIntervention 2009;4:529-33
30) S.R. Chinn et al. “Optical Coherence Tomography using a frequeny tunable optical source.” Opt Lett 1997;22:340-2
31) Ryan TJ, Bauman WB, Kennedy JW, Kereiakes DJ, King SB 3rd, McCallister BD, Smith SC Jr, Ullyot DJ. “Guidelines for percutaneous transluminal coronary angioplasty. A report of the American Heart Association/American College of Cardiology Task Force on Assessment of Diagnostic and Therapeutic Cardiovascular Procedures (Committee on Percutaneous Transluminal Coronary Angioplasty).” Circulation 1993;88:2987–3007.
32) Serruys PW, de Jaegere P, Kiemeneij F, Macaya C, Rutsch W, Heyndrickx G, Emanuelsson H, Marco J, Legrand V, Materne P, et al. “A comparison of balloon-expandable-stent implantation with balloon angioplasty in patients with coronary artery disease.” Benestent Study Group. N Engl J Med 1994;331:489–495.
33) Virmani R, Kolodgie FD, Farb A, Lafont A. “Drug eluting stents: are human and animal studies comparable?” Heart 2003;89:133–138.
34) Farb A, Sangiorgi G, Carter AJ, Walley VM, Edwards WD, Schwartz RS, Virmani R. “Pathology of acute and chronic coronary stenting in humans.” Circulation 1999;99:44–52.
35) Farb A, Weber DK, Kolodgie FD, Burke AP, Virmani R. “Morphological predictors of restenosis after coronary stenting in humans.” Circulation 2002;105:2974–2980.
36) Anderson PG, Bajaj RK, Baxley WA, Roubin GS. “Vascular pathology of balloon-expandable flexible coil stents in humans.” J Am Coll Cardiol 1992;19:372–381.
37) Joner M, Finn AV, Farb A, Mont EK, Kolodgie FD, Ladich E, Kutys R, Skorija K, Gold HK, Virmani R. “Pathology of drug-eluting stents in humans: delayed healing and late thrombotic risk.” J Am Coll Cardiol 2006;48:193–202.
38) Kastrati A, Schomig A, Elezi S, Schuhlen H, Dirschinger J, Hadamitzky M, Wehinger A, Hausleiter J, Walter H, Neumann FJ. “Predictive factors of restenosis after coronary stent placement.” J Am Coll Cardiol 1997;30:1428–1436.
39) Popma JJ, Califf RM, Topol EJ. “Clinical trials of restenosis after coronary angioplasty.” Circulation 1991;84:1426–1436.

40) Lincoff AM, Furst JG, Ellis SG, Tuch RJ, Topol EJ. “Sustained local delivery of dexamethasone by a novel intravascular eluting stent to prevent restenosis in the porcine coronary injury model.” J Am Coll Cardiol 1997;29:808–816.
41) Morice MC, Serruys PW, Sousa JE, Fajadet J, Ban Hayashi E, Perin M, Colombo A, Schuler G, Barragan P, Guagliumi G, Molnar F, Falotico R. “A randomized comparison of a sirolimus-eluting stent with a standard stent for coronary revascularization.” N Engl J Med 2002;346:1773–1780.
42) Moses JW, Leon MB, Popma JJ, Fitzgerald PJ, Holmes DR, O'Shaughnessy C, Caputo RP, Kereiakes DJ, Williams DO, Teirstein PS, Jaeger JL, Kuntz RE. “Sirolimus-eluting stents versus standard stents in patients with stenosis in a native coronary artery.” N Engl J Med 2003;349:1315–1323.
43) Suzuki T, Kopia G, Hayashi S, Bailey LR, Llanos G, Wilensky R, Klugherz BD, Papandreou G, Narayan P, Leon MB, Yeung AC, Tio F, Tsao PS, Falotico R, Carter AJ. “Stent-based delivery of sirolimus reduces neointimal formation in a porcine coronary model.” Circulation 2001;104:1188– 1193.
44) Diaz-Sandoval LJ, Bouma BE, Tearney GJ, Jang IK. “Optical coherence tomography as a tool for percutaneous coronary interventions.” Catheter Cardiovasc Interv. 2005;65(4):492-6.
45) Bouma BE, Tearney GJ, Yabushita H, Shishkov M, Kauffman CR, DeJoseph Gauthier D, MacNeill BD, Houser SL, Aretz HT, Halpern EF, Jang IK. “Evaluation of intracoronary stenting by intravascular optical coherence tomography.” Heart. 2003;89(3):317-20.
46) Jun Tanigawa et al. “Intravascular optical coherence tomography: optimisation of image acquisition and quantitative assessment of stent strut apposition”. EuroInterv.2007;3:128-136.
47) Kaplan AV et al. “Tryton Side-Branch Stent”. EuroIntervention 2006;2:270-271.
48) M. E. Brezinski et al. Circulation 1996 93(6), 1206-13.
49) M. E. Brezinski et al. Am. J. Cardiol. 1996 77, 92-3.
50) E. A. Swanson and C. L. Petersen, Method and Apparatus for High-Speed Longitudinal Scanning in Imaging Systems, U.S. Patent 09/233,421.
51) E. A. Swanson et al. “Ultra-small optical fiber probes and imaging optics” U.S. Patent 09/370,756.
52) Medina et al. “A new classification of coronary bifurcation lesions.” Rev Esp Cardiol 2006;59:183-4
53) Tyczynski et al. “Optical coherence tomography assessment of a new dedicated bifurcation stent.” EuroIntervention. 2009 Nov;5(5):544-51
54) Taniwaga et al. “The influence of strut thickness and cell design on immediate apposition of drug-eluting stents assessed by optical coherence tomography. Int J Cardiol. 2009;134: 180-8
55) Ormiston et al. “Drug-eluting stents for coronary bifurcations: bench testing of provisional side-branch strategies.” Catheter Cardiovasc Interv 2006 Jan;67(1):49-55
56) Ormiston et al. “The “crush” technique for coronary artery bifurcation stenting: insights from micro-computed tomographic imaging of bench deployments.” JACC Cardiovasc Interv. 2008 Aug;1(4):351-7
57) Costa et al. “Bifurcation coronary lesions treated with the “crush” technique: an intravascular ultrasound analysis.” J Am Coll Cardiol. 2005 Aug 16;46(4):599-605

Auteursrechtelijke overeenkomst

Ik/wij verlenen het wereldwijde auteursrecht voor de ingediende eindverhandeling:
New insights with optical coherence tomography in coronary bifurcation lesions treated with the Tryton and Cypher stent

Richting: **master in de biomedische wetenschappen-bio-elektronica en nanotechnologie**
Jaar: **2010**

in alle mogelijke mediaformaten, - bestaande en in de toekomst te ontwikkelen - , aan de Universiteit Hasselt.

Niet tegenstaand deze toekenning van het auteursrecht aan de Universiteit Hasselt behoud ik als auteur het recht om de eindverhandeling, - in zijn geheel of gedeeltelijk -, vrij te reproduceren, (her)publiceren of distribueren zonder de toelating te moeten verkrijgen van de Universiteit Hasselt.

Ik bevestig dat de eindverhandeling mijn origineel werk is, en dat ik het recht heb om de rechten te verlenen die in deze overeenkomst worden beschreven. Ik verklaar tevens dat de eindverhandeling, naar mijn weten, het auteursrecht van anderen niet overtreedt.

Ik verklaar tevens dat ik voor het materiaal in de eindverhandeling dat beschermd wordt door het auteursrecht, de nodige toelatingen heb verkregen zodat ik deze ook aan de Universiteit Hasselt kan overdragen en dat dit duidelijk in de tekst en inhoud van de eindverhandeling werd genotificeerd.

Universiteit Hasselt zal mij als auteur(s) van de eindverhandeling identificeren en zal geen wijzigingen aanbrengen aan de eindverhandeling, uitgezonderd deze toegelaten door deze overeenkomst.

Voor akkoord,

Blomen, Theodorus

Datum: **15/06/2010**